

SCIENTIFIC REPORTS



OPEN

Insights into the role of endonuclease V in RNA metabolism in *Trypanosoma brucei*

Daniel García-Caballero, Guiomar Pérez-Moreno, Antonio M. Estévez, Luis Miguel Ruíz-Pérez, Antonio E. Vidal & Dolores González-Pacanowska

Inosine may arise in DNA as a result of oxidative deamination of adenine or misincorporation of deoxyinosine triphosphate during replication. On the other hand, the occurrence of inosine in RNA is considered a normal and essential modification induced by specific adenosine deaminases acting on mRNA and tRNA. In prokaryotes, endonuclease V (EndoV) can recognize and cleave inosine-containing DNA. In contrast, mammalian EndoVs preferentially cleave inosine-containing RNA, suggesting a role in RNA metabolism for the eukaryotic members of this protein family. We have performed a biochemical characterization of EndoV from the protozoan parasite *Trypanosoma brucei*. *In vitro*, *TbEndoV* efficiently processes single-stranded RNA oligonucleotides with inosine, including A to I-edited tRNA-like substrates but exhibits weak activity over DNA, except when a ribonucleotide is placed 3' to the inosine. Immunolocalization studies performed in procyclic forms indicate that *TbEndoV* is mainly cytosolic yet upon nutritional stress it redistributes and accumulates in stress granules colocalizing with the DEAD-box helicase *TbDhh1*. RNAi-mediated depletion of *TbEndoV* results in moderate growth defects in procyclic cells while the two *EndoV* alleles could be readily knocked out in bloodstream forms. Taken together, these observations suggest an important role of *TbEndoV* in RNA metabolism in procyclic forms of the parasite.

Nucleic acids are continuously exposed to endogenous and environmental damaging agents. Among the most common DNA lesions are nitrogenous base deaminations, which may become a major threat to genetic integrity. Deamination in DNA and RNA can also be enzyme-mediated in a controlled fashion and has an essential role in multiple biological processes^{1–4}. Undesired deamination if not repaired, can give rise to mutations during semi-conservative replicative synthesis, since loss of the amino group changes its pairing properties⁵. For instance, uracil (U), the product of cytosine deamination, pairs with adenine while deaminated adenine or hypoxanthine (Hx) is usually read as G by the DNA polymerase therefore inducing GC > AT and AT > GC transitions respectively. To avoid mutations, these non-canonical bases are mainly removed from DNA by specific DNA glycosylases through the base excision repair (BER) pathway⁶. Early works reported the purification from *E. coli* of an endo-deoxyribonuclease (endonuclease V, EndoV) that also recognizes and nicks DNA containing deaminated bases and therefore could be part of an alternative excision repair (AER) pathway for the elimination of U and Hx from DNA^{7,8}. Besides deaminated bases, EndoV can also cleave an extensive array of damaged DNA lesions including AP sites, mismatched base pairs and flap and pseudo-Y DNA structures^{8–14}. In spite of its broad substrate specificity, biochemical and genetic evidences led to conclude a preferential role in the repair of deoxyinosine (the deoxynucleoside containing Hx) in double- and single-stranded DNA^{8,15,16}. In both cases, EndoV catalyzes the cleavage of the second phosphodiester bond 3' to the lesion without releasing the erroneous nucleotide¹⁴. Hence, additional enzymatic factors are required to eliminate the lesion and complete the repair although they have not been yet identified. *In vitro*, purified DNA polymerase I and DNA ligase appear sufficient to reconstitute the repair process^{17,18}.

EndoV homologues are widely conserved throughout bacteria, archaea and eukaryotes but with differences in substrate specificity that likely imply some degree of divergence in their cellular functions. Although *E. coli* EndoV has been described as a DNA repair enzyme for many years, in fact, it can also act on inosine at RNA with

Departamento de Bioquímica y Farmacología Molecular, Instituto de Parasitología y Biomedicina Lopez-Neyra, Consejo Superior de Investigaciones Científicas (CSIC), Armilla (Granada), 18016, Spain. Correspondence and requests for materials should be addressed to A.E.V. (email: avidal@ipb.csic.es) or D.G.-P. (email: dgonzalez@ipb.csic.es)

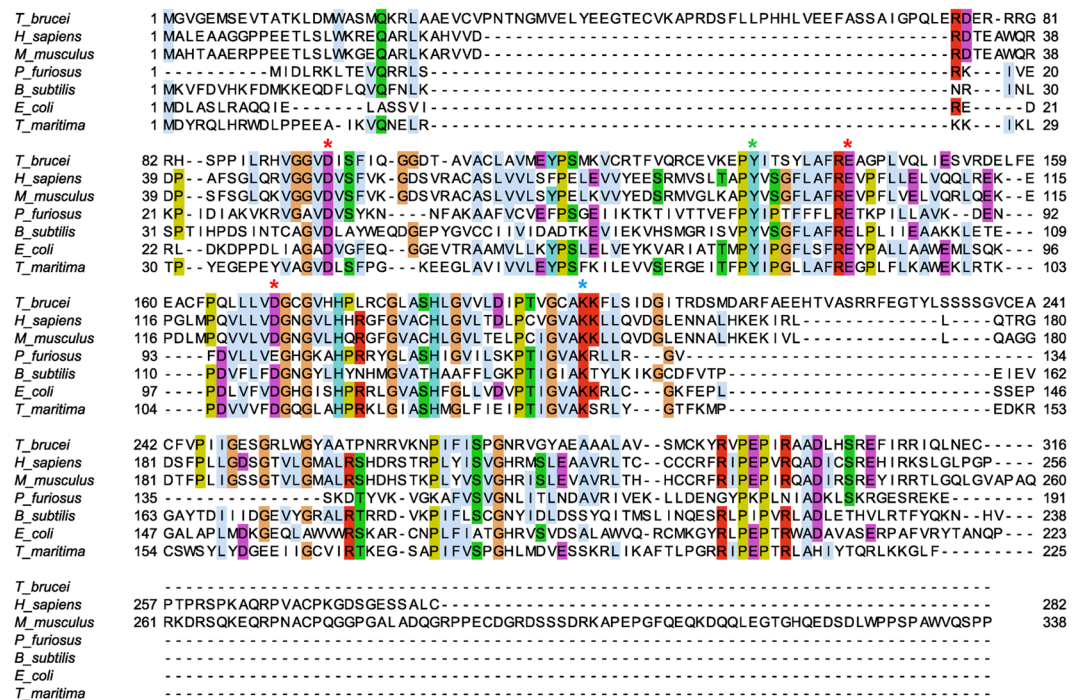


Figure 1. Sequence alignment of endonuclease V orthologs from several organisms including *T. brucei*. The alignment was made in ClustalOmega and visualized with JalView. Amino acids are colored using the clustal color scheme (for more details check the following web page: <http://www.jalview.org/help/html/colourSchemes/clustal.html>) and the identity threshold was set at 50%. The amino acids involved in metal cofactor interaction are indicated by red asterisks, the amino acids responsible for substrate-enzyme interaction are indicated by green asterisks and the amino acids involved in product-enzyme interaction are marked with blue asterisks. Protein sequences were retrieved from NCBI RefSeq: *T. brucei*, *Trypanosoma brucei* (XP_822927.1); *H. sapiens*, *Homo sapiens* (NP_775898.2); *M. musculus*, *Mus musculus* (NP_001158108.1); *P. furiosus*, *Pyrococcus furiosus* (AFN03782.1); *B. subtilis*, *Bacillus subtilis* (NP_391498.2); *E. coli*, *Escherichia coli* (NP_418426.2); *T. maritima*, *Thermotoga maritima* (NP_229661.1).

equal efficiency¹⁹. Similarly, the enzyme of the *Pyrococcus furiosus* archaeon shows strong activity toward RNA substrates as well as DNA substrates²⁰. In contrast, mouse and human EndoVs exhibit very weak activity over deoxyinosine and DNA substrates in general^{21,22} whereas they incise inosine-containing RNA very efficiently, suggesting a role in RNA metabolism instead of DNA repair for the mammalian enzymes^{19,23,24}.

Trypanosoma brucei is a protozoan parasite belonging to the Kinetoplastida order and the causative agent of African trypanosomiasis and nagana in humans and animals, respectively²⁵. During its life cycle, *T. brucei* alternates between an insect and a mammalian host and the adaptation to the environmental conditions requires significant structural and physiological changes. During infection, an essential component of the primary immune response is the production of nitric oxide (NO) by activated phagocytes that generates reactive oxygen and nitrogen species (ROS and RNS). However, the impact of DNA repair mechanisms such as endonuclease V to counteract host-generated oxidative and nitrosative stress has not been yet investigated in these human pathogens and may be relevant to understand their capacity to survive in such adverse environment. Here, we have purified and characterized the catalytic properties of the endonuclease V encoded by *Trypanosoma brucei* genome (*TbEndoV*). *In vitro*, *TbEndoV* efficiently processes inosine-containing single-stranded RNA oligonucleotides, including A to I-edited tRNA-like substrates. On the contrary, a weak activity was observed over inosine in DNA, except when a ribonucleotide was placed 3' to the lesion. Analysis by immunofluorescence microscopy indicates that *TbEndoV* localizes predominantly to the cytosol. The enzyme appears to be non-essential in bloodstream forms (mammalian-stage parasites) where the two *EndoV* alleles could be readily knocked out. In contrast, protein depletion in procyclic forms (insect-stage parasites) by RNA interference led to impaired growth and defects in cell cycle progression, thus suggesting a specific and vital role for *TbEndoV* at this life stage.

Results

Identification of a putative endonuclease V in *Trypanosoma brucei*. Homology searching of the *Trypanosoma brucei* genome database, using the human endonuclease V ortholog as the query sequence, identified a protein annotated as a putative endonuclease V (Tb927.10.6860) composed of 316 amino acids and a calculated mass of 34.9 kDa. The *T. brucei* EndoV protein sequence was aligned with other six characterized orthologs from prokaryotic and eukaryotic organisms (Fig. 1). Three amino acids identified as crucial for endonuclease activity in *Thermotoga maritima*, Asp43, Glu89 and Asp110, are conserved in *TbEndoV*. These residues

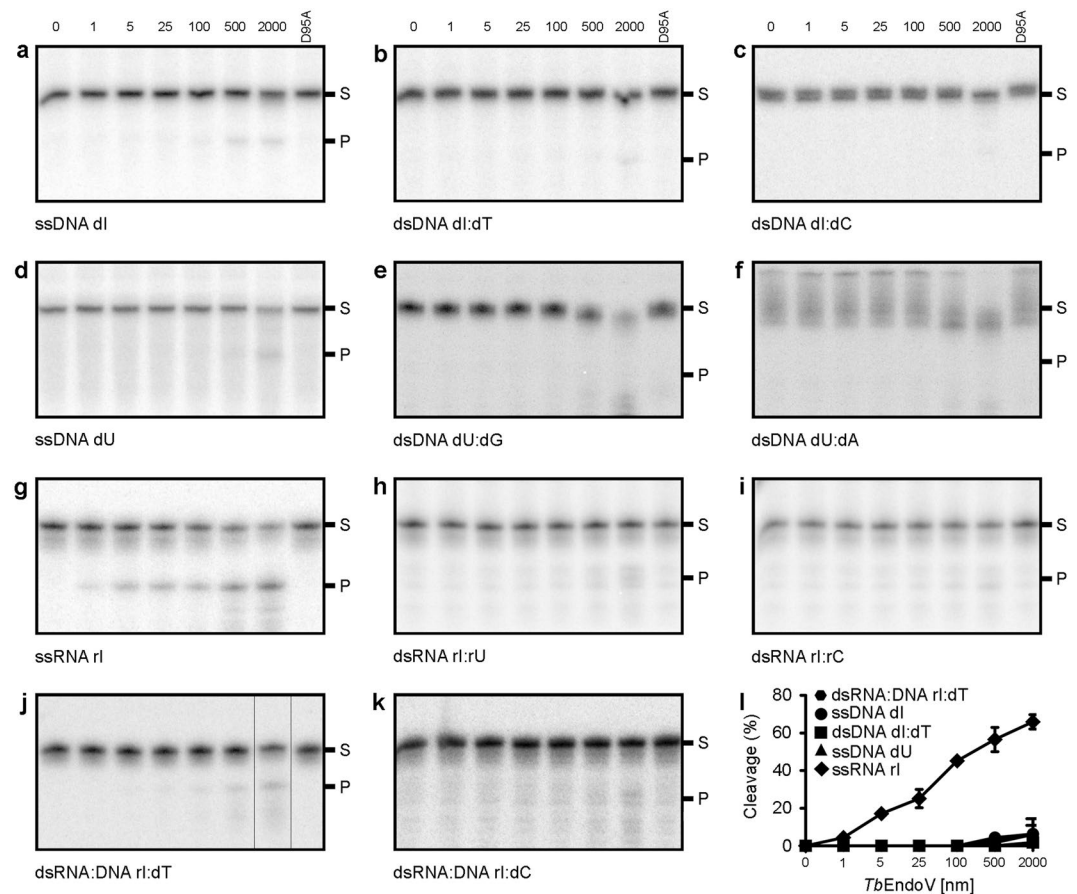


Figure 2. *TbEndoV* acts efficiently upon inosine-containing ssRNA. DNA substrates with (a–c) inosine or (d–f) uracil, and (g) single and (h,i) double-strand RNA substrates or (j,k) RNA–DNA hybrids were incubated with increasing amounts of *TbEndoV* (0–2000 nM, as indicated). (l) Plot of the percentage of substrate cleaved by endonuclease V activity versus the total amount of protein used in the reaction. Each point represents the mean (\pm s.d.) from three independent experiments. The D95A catalytic mutant was used as negative control. Reaction products were analyzed by 20% denaturing PAGE. Image in j was cropped and edited for easier comparison. Positions of the reaction substrate (S) and product (P) are indicated.

coordinate the interaction with the metal cofactor which is essential for catalysis²⁶. Sequence comparison revealed that, *TbEndoV* exhibits a high similarity to the human ortholog (identity = 37%; $E = 3 \times 10^{-41}$; bits = 143).

***T. brucei* endonuclease V preferentially cleaves inosine-containing RNA.** To characterize the enzymatic properties of *TbEndoV*, the corresponding open reading frame was amplified by PCR and cloned into an *E. coli* vector that allows expression of the protein fused to the maltose-binding protein in order to increase its expression and solubility. The MBP-*TbEndoV* protein was overexpressed in the *E. coli* TB1 strain and purified to over 99% purity by amylose affinity and gel filtration chromatography.

The purified recombinant protein was initially assayed for endonuclease activity on 5'-radiolabeled 21-nucleotide single- and double-strand DNA substrates in which one strand contained hypoxanthine or uracil in a central position. Oligonucleotide sequences can be found in Fig. S1. Double-strand substrates were designed to produce Hx:T (dsDNA dI:dT), Hx:C (dsDNA dI:dC), U:G (dsDNA dU:dG) and U:A (dsDNA dU:dA) base pairs that mimic potentially physiological DNA substrates. The dsDNA dI:dT and dsDNA dU:dG substrates may result from adenine and cytosine deamination at A:T and C:G base pairs respectively while dsDNA dI:dC and dsDNA dU:dA can be generated during replicative synthesis of hypoxanthine- or uracil-containing DNA strands, respectively. In general, *TbEndoV* showed poor or no endonuclease activity on these DNA substrates (Fig. 2a–f). Indeed, ssDNA dI and dsDNA dI:dT were only cleaved at very high enzyme concentrations while practically no cleavage was observed with dsDNA dI:dC (Fig. 2a–c). The trypanosomal enzyme also exhibits residual activity on uracil in ssDNA substrates while no activity was detected over the uracil-containing dsDNA substrates (Fig. 2d–f). To rule out a possible contamination with bacterial endonuclease V during purification, we generated a D95A catalytic mutant by site-directed mutagenesis. The aspartate at this position is a highly conserved residue responsible for the coordination of the metal cofactor during substrate cleavage²⁷. As shown in Fig. 2, replacement of aspartate 95 by alanine fully abolished *TbEndoV* activity in agreement with studies on homologous enzymes^{19, 28, 29}. Hence, the activity detected is intrinsic to *TbEndoV*.

While bacterial EndoV cleaves both DNA and RNA substrates, the human enzyme has been reported to act more efficiently upon inosine-containing RNA substrates^{19,23}. Indeed, riboinosine can arise by spontaneous or chemically-induced adenine deamination, as a consequence of enzymatic RNA-editing or by erroneous incorporation of ITP during transcription³⁰. We therefore tested the activity of *Tb*EndoV using different RNA substrates (Fig. 2). As shown in Fig. 2g, trypanosomal EndoV efficiently cleaves single-strand RNA substrates with inosine (ssRNA rI) but is not able to process double-strand RNA when Hx pairs with U (dsRNA rI:rU) or cytosine (dsRNA rI:rC) (Fig. 2h,i). As expected, the incubation of the RNA substrates with the D95A catalytic mutant did not result in product formation.

We have also considered the possibility that riboinosine could be incorporated into nascent RNA during transcription giving rise to a transient RNA:DNA hybrid where Hx would establish a stable base pair with C. However, the cleavage assay did not reveal significant endonuclease activity using the dsRNA:DNA rI:dC substrate and only minor incision was detected with a similar substrate containing an Hx:T mispair (dsRNA:DNA rI:dT) (Fig. 2j,k).

Once ssRNA rI was established as the preferred substrate for *Tb*EndoV (Fig. 2l), reaction conditions were empirically varied to determine how they affected its incision activity (Fig. S2). We found that *Tb*EndoV acts more efficiently at pH 7.5 when using 1 mM MnCl₂, the preferred metal cofactor (Fig. S2a,c). On the other hand, addition of high concentrations of NaCl or KCl (≥ 100 mM) greatly inhibited *Tb*EndoV activity and therefore, salts were not included in the final reaction buffer (Fig. S2b). We also noticed that the ssRNA rI substrate was refractory to undergo complete cleavage by *Tb*EndoV even at high enzyme concentrations and under different reaction conditions tested. In contrast, total incision was achieved with an alternative substrate sequence, indicating that substrate recognition and/or incision is sequence-dependent and activity could be influenced by the secondary structure of the substrate (Fig. S2d).

Analysis of the substrate determinants for the inosine recognition and cleavage. Both mammalian and prokaryotic EndoVs recognize inosine and cleave at the second phosphodiester bond 3' to the lesion^{14,19,20}. However, while human and mouse enzymes act only upon RNA, bacterial EndoV operates efficiently on DNA and RNA. The strong preference of trypanosomal EndoV for inosine in RNA suggests that the 2' hydroxyl group of the ribose is required for an efficient catalysis. Here, we have investigated the effect of specific substrate determinants on *Tb*EndoV catalytic function. A set of DNA oligonucleotides was designed to examine how the presence of a ribose either at the lesion site or at the 3'-adjacent nucleotide affected the incision of *in situ* deamination products. As shown in Fig. 3, DNA substrates (ssDNA rIdG and dsDNA rIdG:dTdC) containing a riboinosine but followed by a deoxyribose are not efficiently cleaved by *Tb*EndoV (Fig. 3a,b,e). However, when a ribonucleotide is placed at the 3' position of a deoxyinosine lesion, *Tb*EndoV incision activity is greatly enhanced, regardless the DNA substrate is single (ssDNA dIrG) or double-stranded (dsDNA dIrG:dTdC) (Fig. 3c,d,e).

***Tb*EndoV acts upon tRNA substrates containing inosine.** RNA-editing is a potential source of inosine in trypanosomes since ADAT proteins have been characterized in these organisms^{4,31}. In particular, threonine coding tRNA showed high editing levels at positions 32 (C-to-U editing) and 34 (A-to-I editing) in *T. brucei*⁴. To determine whether this could be a biologically relevant RNA substrate, we assayed the *Tb*EndoV incision activity over non-edited, single- and double-edited tRNA-mimicking substrates (Fig. 4). As expected, *Tb*EndoV did not cleave the non-edited (Fig. 4a,e) or the C to U edited substrates with adenine at position 34 (Fig. 4c,e). In contrast, the tRNA containing Hx at position 34 (C₃₂I₃₄) was efficiently processed *in vitro* (Fig. 4b,e) and could be a potential cellular target for endonuclease V in *T. brucei*. Notably, the additional presence of U at position 32 had a negative impact on the endonuclease ability to cleave this tRNA substrate (U₃₂I₃₄), suggesting that cytosine deamination at position 32 may act as an inhibitory mechanism to prevent the processing of A to I-edited tRNAs by EndoV.

Subcellular localization of *Tb*EndoV. Endonuclease V has been localized to the cytosol of human cells²³ but also associated to the nucleoli³². In order to determine the subcellular localization of the parasite enzyme, specific rabbit polyclonal antibodies against *Tb*EndoV were raised using soluble recombinant His-*Tb*EndoV as antigen. To ensure higher specificity, antibodies were purified from blood serum by affinity chromatography against the same pure recombinant protein. Immunoblotting analysis failed to detect EndoV protein in procyclic and bloodstream whole cell extracts, even though the antibody does react efficiently with twenty nanograms of purified recombinant protein (Fig. 5a), suggesting that EndoV expression levels are extremely low in trypanosomes. To overcome this limitation for subcellular localization studies, we generated procyclic *T. brucei* cell lines stably overexpressing *Tb*EndoV (PF/*Tb*EndoV) or a C-terminal Myc-tagged version of *Tb*EndoV (PF/*Tb*EndoV-myc). Protein levels were monitored using the purified anti-*Tb*EndoV and monoclonal anti-myc antibodies, respectively (Fig. 5b,c). Both, polyclonal and monoclonal antibodies, recognize a single and highly intense band in western blots. In spite of the high levels of protein synthesis, *Tb*EndoV overexpression did not appear to have any impact on proliferation and therefore these transgenic cells were considered suitable for cellular localization studies.

Immunofluorescence microscopy images obtained from the parental procyclic cell line (PF) (Fig. 5d, upper row) and the *Tb*EndoV-overexpressing cell line (middle row) revealed a granular staining pattern with predominant localization in the cytosol and at a much lesser extent in the nucleus. The same distribution pattern was verified in an independent experiment using a monoclonal anti-myc antibody on PF/*Tb*EndoV-myc cells (Fig. 5d, lower row). These results demonstrate that *Tb*EndoV performs an important function in the cytoplasm although a certain role in the nucleus cannot be excluded. Our analysis provides the first experimental evidence of the subcellular localization of a eukaryotic EndoV under endogenous expression conditions, avoiding this way potential overexpression-induced artifacts.

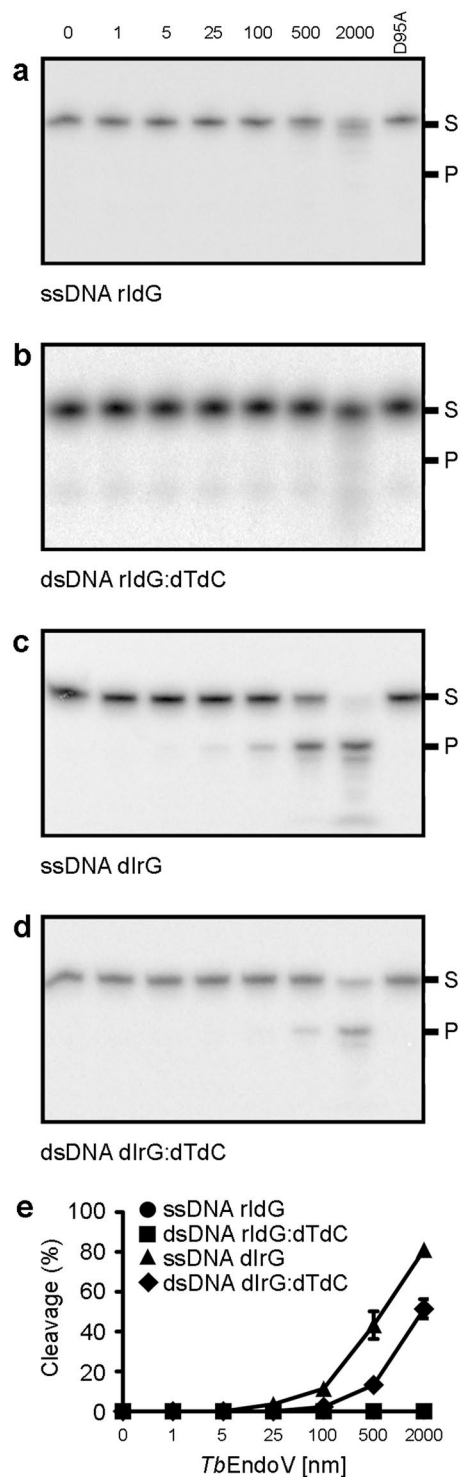


Figure 3. Analysis of substrate determinants for the incision activity of *TbEndoV*. DNA substrates with (a,b) riboinosine or (c,d) a ribonucleotide located 3' to the inosine lesion were incubated with increasing amounts of *TbEndoV* (0–2000 nM, as indicated). (e) Plot of the percentage of substrate cleaved by endonuclease V activity versus total amount of protein used in the reaction. Each point represents the mean (\pm s.d.) from three independent experiments. The D95A catalytic mutant was also included as control. Reaction products were analyzed by 20% denaturing PAGE. Positions of the reaction substrate (S) and product (P) are indicated.

***TbEndoV* depletion impairs proliferation of *T. brucei* procyclic forms.** In order to assess whether *T. brucei* requires the EndoV activity for normal proliferation and survival, we proceeded to generate *EndoV*-null mutants in bloodstream and procyclic forms of the parasite. For bloodstream forms, replacement cassettes

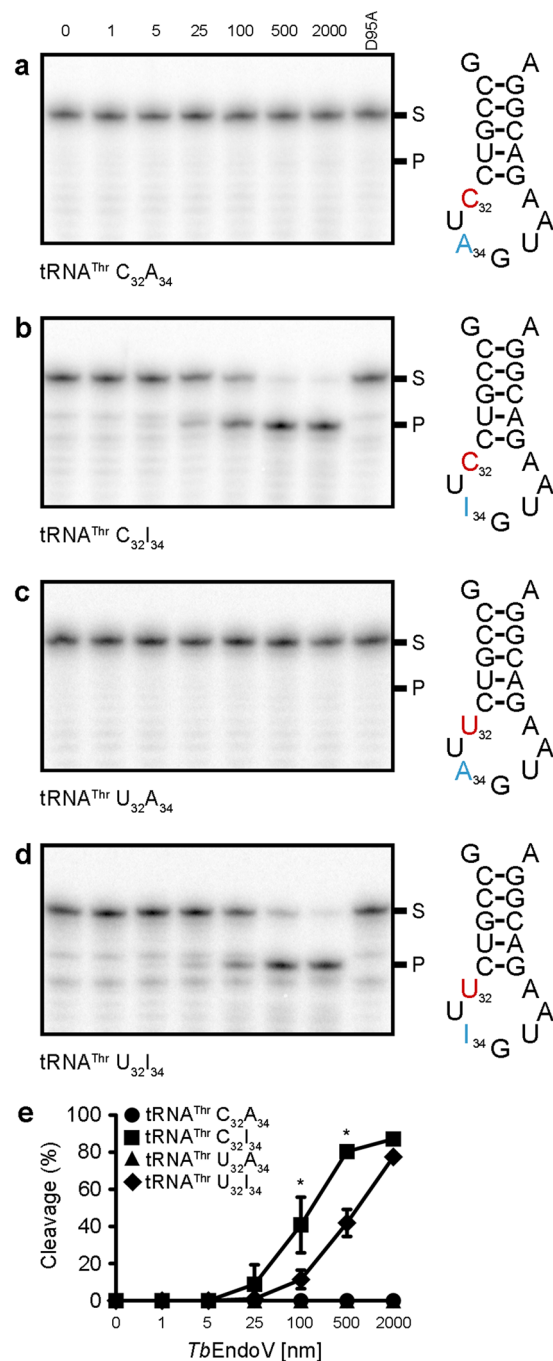


Figure 4. *TbEndoV* can process tRNA-mimicking substrates containing inosine. Two positions (cytosine 32 and adenine 34) undergo editing in threonine-coding tRNAs in *T. brucei*⁴. To replicate the edited substrates, bases corresponding to C32 and A34 were substituted by their corresponding deamination products, uracil and hypoxanthine respectively. Substrates were incubated with increasing amounts of *TbEndoV* (0–2000 nM, as indicated). (a) Control non-edited substrate; (b) adenine-edited substrate; (c) cytosine-edited substrate and (d) double-edited substrate. (e) Quantification of the data from (a–d). Each point represents the mean (\pm s.d.) from three independent experiments. The asterisks show significant differences calculated by a two-tailed Student's t-test: * $p < 0.05$. Reaction products were analyzed by 20% denaturing PAGE. Positions of the reaction substrate (S) and product (P) are indicated.

contained a puromycin-resistance gene (*PAC*) and a phleomycin-resistance gene (*BLE*), flanked by 550 bp of the *EndoV* 5'-UTR and 3'-UTR sequences (Fig. S3). All DNA fragments were obtained by PCR amplification of *T. brucei* 427 genomic DNA and primers were designed from the sequence obtained from the GeneDB database. Linear targeting fragments containing each of the inactivation cassettes were initially transfected into *T. brucei* bloodstream strain yielding recombinant clones, which were efficiently isolated in selective media with puromycin or phleomycin. One of the puromycin-resistant clones was subjected to a second round of inactivation

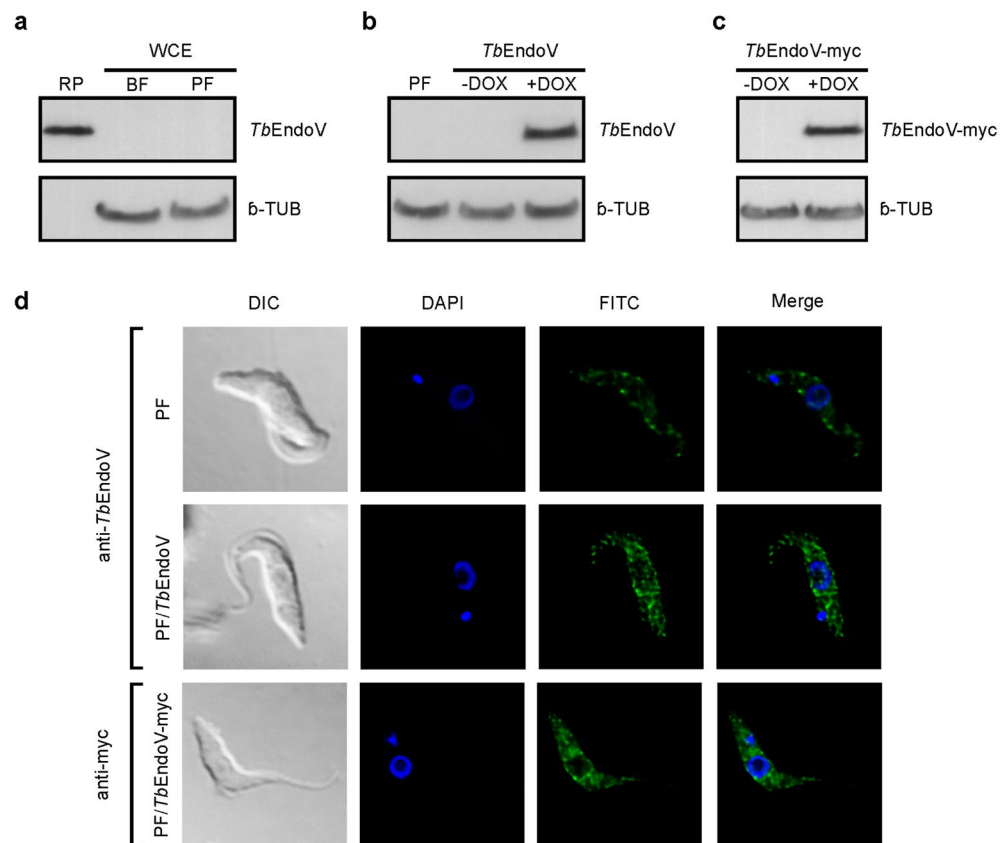


Figure 5. Subcellular localization of endonuclease V in *T. brucei* cells. **(a)** Analysis by western blot of the expression levels of EndoV in bloodstream (BF) and procyclic (PF) forms using an anti-*TbEndoV* polyclonal antibody generated in our laboratory. Recombinant purified *TbEndoV* (20 ng) (RP) was included as positive control. **(b)** Expression of native *TbEndoV* and **(c)** *TbEndoV*-myc was detected in doxycycline induced *TbEndoV*- and *TbEndoV*-myc-overexpressing PF cells using the anti-*TbEndoV* polyclonal antibody or an anti-myc monoclonal antibody, respectively. Anti- β -tubulin was used as loading control in all western blotting analysis. **(d)** Immunofluorescence microscopy analysis showing the subcellular localization of *TbEndoV*. Parental cell line (PF) (upper row), *TbEndoV*- (middle row) and *TbEndoV*-myc-overexpressing PF cells (lower row).

with the *BLE* cassette obtaining this way transfectants resistant to puromycin and phleomycin. Integration of the *PAC* or *BLE* markers was monitored by PCR using primers that hybridize with the flanking genes upstream and downstream from the *TbEndoV* gene in combination with marker-specific primers (Fig. S3). As expected, no expression of *TbEndoV* mRNA was observed by RT-PCR in the selected clone (Fig. 6a). Despite lacking *TbEndoV*, double knockout cells exhibited similar proliferation rate as parental cells (Fig. 6b), providing direct evidence that the enzymatic activity of *TbEndoV* is not essential for viability or proliferation of bloodstream trypanosomes *in vitro*.

Inactivation of *TbEndoV* by homologous recombination was also attempted in procyclic *T. brucei* cells; however, two-allele replacement could not be achieved after several attempts. We therefore used an alternative knock-down approach that allows monitoring the cellular events that follow the reduction of EndoV activity. We therefore proceeded to silence *TbEndoV* expression using the RNA interference (RNAi) methodology. Due to the low constitutive expression of *TbEndoV*, we monitored the inhibition of expression using qRT-PCR. As shown in Fig. 6c, *TbEndoV* could be successfully depleted in doxycycline-induced RNAi-transfected cells. Determination of the *TbEndoV* mRNA levels at two, four and six days after doxycycline addition revealed a decrease of 25%, 60% and 49% respectively, in comparison to the parental strain. A time course analysis of parasite growth was carried out during 16 days to determine the effect of *TbEndoV* depletion. Cells where *TbEndoV* was down-regulated exhibited a moderate but consistent defect in proliferation with respect to non-induced or parental control cells (Fig. 6d).

EndoV-deficient cells were further analyzed by quantifying the DNA content by flow cytometry together with DAPI staining of nuclei and kinetoplasts. FACS analysis revealed a significant increase of EndoV-deficient trypanosomes in the S-phase (Fig. 6e), which is consistent with the accumulation of cells with an enlarged kinetoplast (1N1K*) observed in cells that have already initiated nuclear DNA duplication (Fig. 6f,g). At the same time, cells in which EndoV was knocked-down also displayed a decrease in 1N1K (corresponding to cells in G1) and a concomitant increase in the population of 1N2K cells (G2 phase) (Fig. 6e,f). The major anomaly was the presence

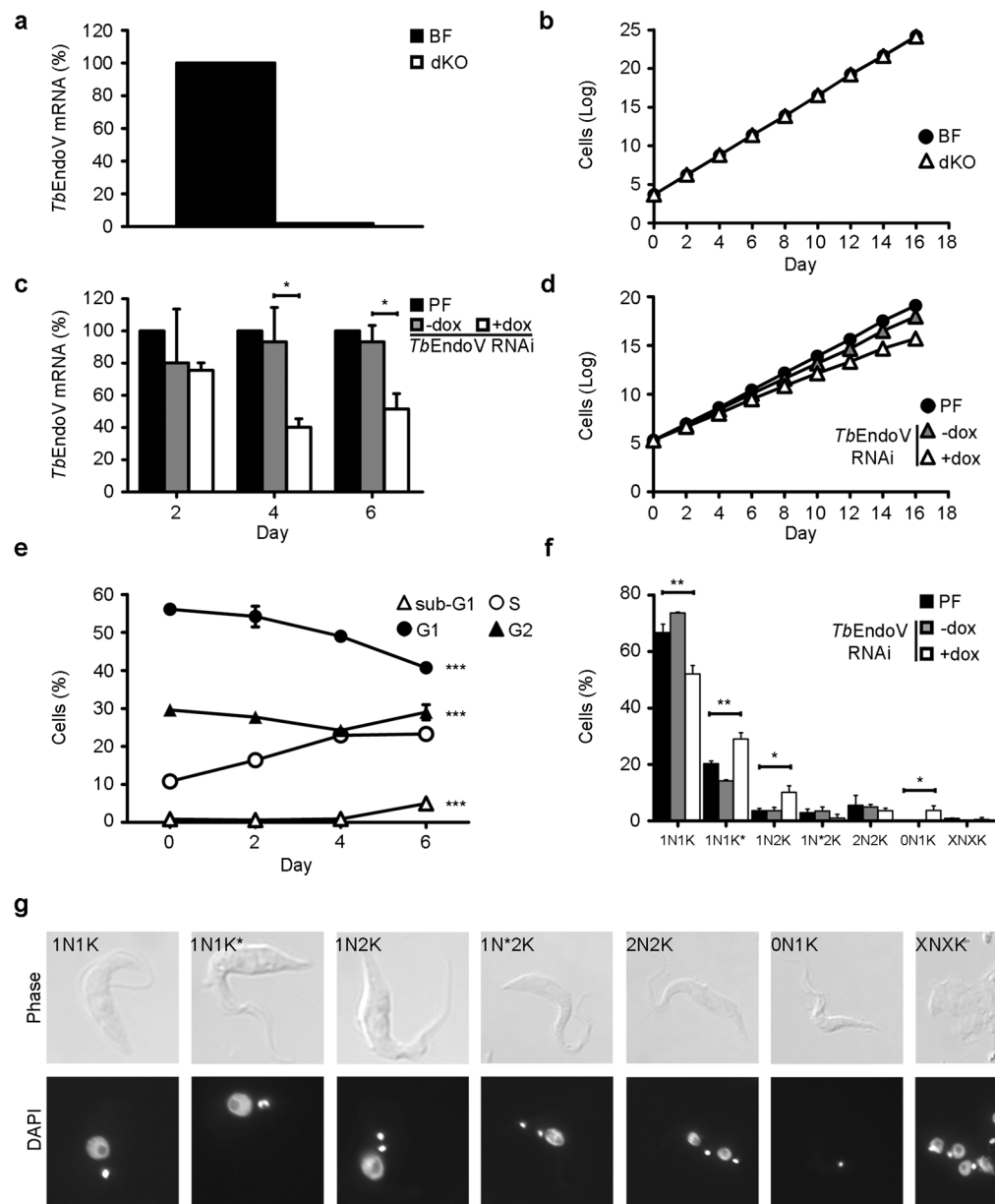


Figure 6. Characterization of *T. brucei* cell lines defective in endonuclease V. **(a,b)** *TbEndoV* was knocked-out in bloodstream *T. brucei* cells. **(a)** *TbEndoV* mRNA levels and **(b)** proliferation curve are shown. **(c,d)** *TbEndoV* depletion in procyclic *T. brucei* by RNA interference. **(c)** *TbEndoV* mRNA levels were monitored by quantitative-PCR at different time points after RNAi induction. qRT-PCR data correspond to the mean (\pm s.d.) of three samples from three independent experiments. The asterisks show significant differences calculated by a two-tailed Student's t-test: * $p < 0.05$. **(d)** Plots showing the proliferation curves after RNAi induction. **(e)** Cell cycle progression was analyzed during a time course of 6 days using FACS in *TbEndoV*-RNAi cells induced with $1 \mu\text{g}\cdot\text{mL}^{-1}$ of doxycycline. Data correspond to the mean (\pm s.d.) of two samples coming from three independent experiments. Two-tailed Student's t-test was calculated for differences between day 0 and 6 (** $p < 0.001$) **(f)** Quantification of nuclei (N) and kinetoplasts (K) in parental and *TbEndoV*-RNAi cells after 6 days of induction with $1 \mu\text{g}\cdot\text{mL}^{-1}$ of doxycycline. Data correspond to mean percentages (\pm s.d.) of total cells (>300) coming from three independent experiments. The asterisks show significant differences calculated by a two-tailed Student's t-test: * $p < 0.05$, ** $p < 0.01$, *** $p < 0.001$. **(g)** Representative fluorescence microscopy images of *TbEndoV*-deficient cells at day 6 post-RNAi induction. Parasite morphology (Phase) and the number of nuclei (N) and kinetoplasts (K) are shown (DAPI staining). N* indicates an enlarged nucleus and K* an enlarged kinetoplast.

of cells with one kinetoplast but without nucleus (0N1K), also known as zoids (Fig. 6f,g), that may account for the sub-G1 population detected by flow cytometry. Similar cell phenotypes have been described in procyclic *T. brucei* cells after treatment with aphidicolin or bleomycin where the inhibition of nuclear S phase was followed by defective mitosis^{33,34}.

TbEndoV localizes to stress granules after starvation. Human EndoV has been shown to relocate to cytoplasmic RNA-containing granules in response to cellular stress caused by sodium arsenite where it could be contributing to the elimination of damaged inosine-containing transcripts²⁴. Stress granules (SGs) are transient aggregates of stalled translation initiation complexes whose function is to preserve the mRNAs and prevent their translation until the normal conditions are restored. Oxidative stress, glucose deprivation, heat-shock, viral infections etc. are demonstrated inducers of stress granule formation³⁵. In trypanosomes, SGs have been observed in the procyclic forms that have to cope with periods of starvation and temperature changes inside the insect³⁶. To address whether *TbEndoV* might be relocating in SGs after starvation-induced stress, cells were cultured in carbon-free buffer (PBS) for different time periods and subsequently monitored by fluorescence microscopy (Fig. 7a). After 120 min in PBS, endogenous *TbEndoV* protein accumulated into discrete *foci* which were bigger in size than the granule particles observed in cells grown in normal rich medium (untreated) (Fig. 7c). Under the same conditions, the DEAD-box RNA helicase *TbDhh1*, a well-characterized component of starvation SGs³⁷, also relocates into *foci* although with different kinetics, thus validating the protocol used to induce starvation (Fig. 7a). To validate the specificity of the signal detected, cells where *TbEndoV* expression was silenced by RNAi were analyzed by immunofluorescence microscopy (Fig. 7b). Quantitative analysis revealed that trypanosomes expressing low levels of *TbEndoV* exhibited a significant reduction in the number and size of *TbEndoV*-positive granules after 120 min in the absence of a carbon source thus confirming the specific accumulation of this endonuclease in starvation-induced granules (Fig. 7c).

We next proceeded to establish whether *TbEndoV* does actually colocalize with the RNA-binding protein *TbDhh1* in SGs upon starvation. To perform the colocalization experiments, the anti-*TbEndoV* antibody was non-covalently labeled with Alexa Fluor® 594 while the polyclonal anti-*TbDhh1* was detected with an Alexa Fluor® 488-conjugated secondary anti-rabbit antibody. Immunostaining showed extensive colocalization of *TbEndoV* and *TbDhh1* granules at 120 minutes after induction of starvation (Fig. 7d). Pearson's correlation and Manders' overlap coefficients were determined to establish the degree of colocalization. Manders' coefficient indicate that 74% of the signal corresponding to *TbDhh1* overlaps with *TbEndoV* ($M1 = 0.74 \pm 0.13$) and *vice versa*, 70% of *TbEndoV* fluorescence overlaps with *TbDhh1* ($M2 = 0.70 \pm 0.11$). The colocalization is also supported by the Pearson's correlation coefficient (0.87 ± 0.04). These data demonstrate the presence of *TbEndoV* in SGs and a role for this protein in the stress response to starvation.

Discussion

Trypanosoma brucei is an extracellular parasite under constant exposure to oxidative and nitrosative stress either generated as a byproduct of its own metabolism or produced by immune effector cells in response to parasite infection^{38,39}. It is well established that ROS and RNS can damage vital molecules, such as proteins, lipids, or nucleic acids⁴⁰. Therefore, protozoan survival and genomic stability greatly depends on DNA repair systems, which for that reason could be excellent targets for chemotherapeutic interventions⁴¹.

Deaminated DNA bases such as uracil and hypoxanthine arise as result of spontaneous hydrolysis or induced by oxidative or nitrosative agents. These lesions are the substrate of specialized DNA glycosylases as part of the BER system, which carries out the correction of DNA alterations that do not distort the overall structure of DNA helix. *T. brucei* expresses a single uracil-DNA glycosylase activity (UNG)⁴² responsible for excision of U but no glycosylases with capacity to excise Hx, generally an alkylpurine-DNA glycosylase⁴³, have been identified in kinetoplastid parasites⁴⁴. While in bacteria, EndoV provides a back-up mechanism for the repair of Hx and U⁴⁵, trypanosomal EndoV is not endowed with significant activity over DNA substrates and therefore it is unlikely that this enzyme performs an important role in DNA repair. Nevertheless, we cannot exclude the possibility that neglected factors in our *in vitro* cleavage assay may enhance the enzyme activity over DNA *in vivo*. Similarly to mammalian EndoVs which have been associated to a possible role in RNA processing^{19,23}, *TbEndoV* exhibits strict specificity for inosine in RNA suggesting that this might be the potential *bona fide* substrate in physiological conditions.

Several potential biological targets can be anticipated for *TbEndoV*. Deamination of adenine can occur in RNA and their precursors via hydrolytic and nitrosative reactions upon exposure to endogenous or exogenous agents⁴⁶. *T. brucei* is exposed to RNS in the early steps of an infection, after nitric oxide (NO) and ROS are released by phagocytes as part of the primary immune response⁴⁷. RNS can react with nucleic acids generating strand breaks and base modifications including deaminations⁴⁸, which constitute the primary cause of NO-induced mutagenicity in a variety of organisms^{49,50}. The nucleotide pool may also undergo base deaminations under the same circumstances leading to the generation of non-canonical ITP that could be erroneously incorporated by the RNA polymerase during transcription. Supporting this notion, *E. coli* and yeast cells defective in inosine triphosphate pyrophosphatase (ITPase) exhibit increased levels of inosine in their RNA⁵¹. The presence of Hx in mRNAs could have mutagenic consequences during gene expression since it is recognized as guanine during protein translation⁵. Likewise, the presence of inosine in tRNAs and rRNAs might modulate or interfere with protein translation as described for other modifications⁵². Recognition and cleavage by EndoV endonuclease activity of adenine-deaminated transcripts would prevent the formation of mutant proteins thus acting as a mechanism to eliminate potentially harmful mRNAs.

Another source of inosine in RNA relies on the enzymatic activity of specific adenosine deaminases acting on mRNA (ADAR) and tRNA (ADAT)¹. These enzymes play an important role introducing inosine in specific positions of RNA, a key process for correct splicing and codon diversity⁵³. While no ADAR protein has been identified in *T. brucei*, adenine deamination in tRNAs by ADAT enzymes has been extensively described^{4,31}. In particular, a heterodimer made up of two subunits (ADAT2 and ADAT3) is responsible for specific A to Hx deamination³ in *T. brucei*. Eight different tRNA species (for Ala, Arg, Ile, Leu, Pro, Ser, Thr and Val amino acids) have adenine at the wobble position of the anticodon and therefore, potential A-to-I editing sites. Indeed, threonine coding tRNA is highly edited at position 34 (A-to-I) but also at position 32 (C-to-U) in *T. brucei*⁴. *In vitro*, *TbEndoV* cleaves the trypanosomal A-to-I edited tRNA substrates with high efficiency, suggesting that the turnover of edited tRNAs

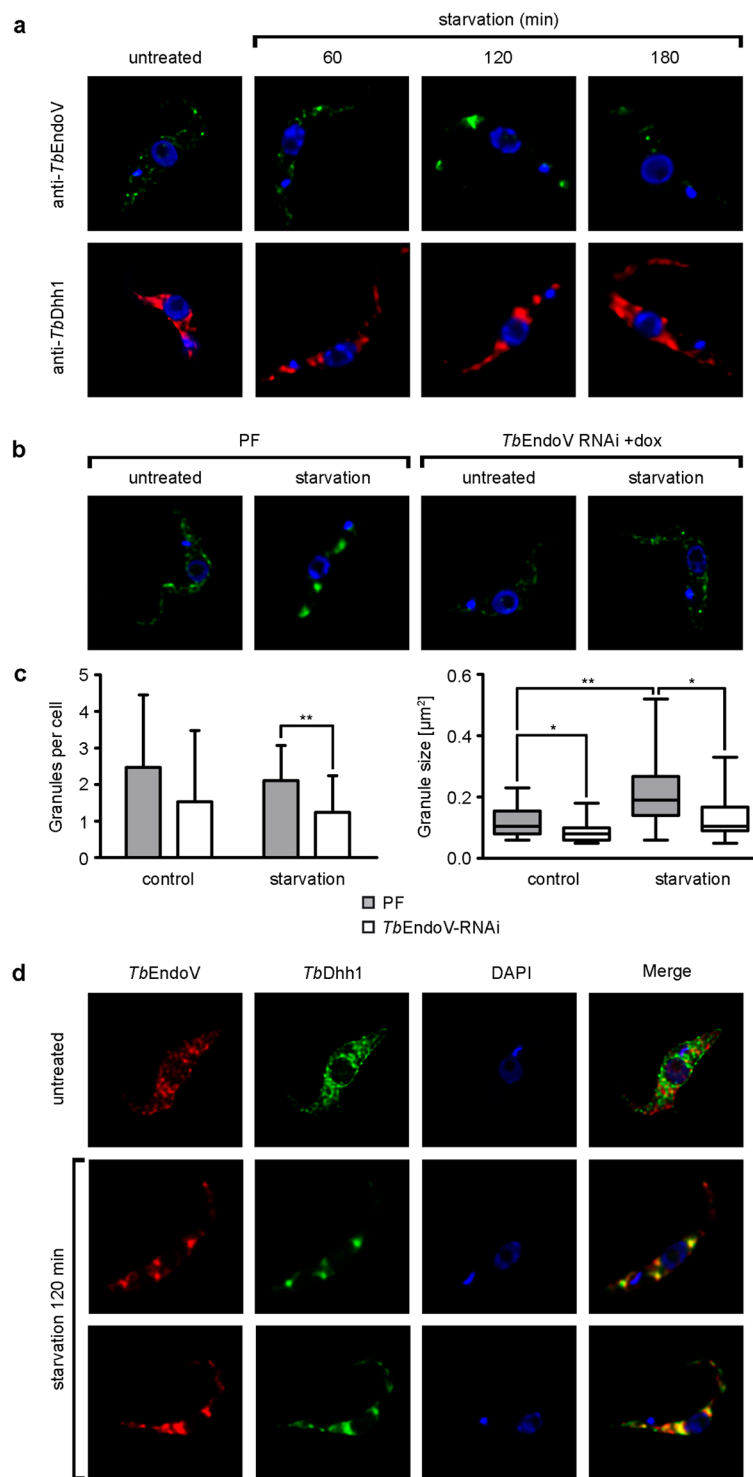


Figure 7. *TbEndoV* relocalizes into cytoplasmic granules upon nutritional stress. **(a)** To induce nutritional stress, trypanosomes were washed and maintained in PBS for different time periods as indicated prior to fixation, and then processed for single immunofluorescence staining using the following pairs of primary and secondary antibodies: rabbit anti-*TbEndoV*/Alexa Fluor[®] 488-conjugated goat anti-rabbit IgG or rabbit anti-*TbDhh1*/Alexa Fluor[®] 488-conjugated goat anti-rabbit IgG. Untreated (no exposure to PBS) cells were used as control. Nuclear DNA and the kinetoplast were visualized by DAPI staining. The images were representative of each staining from at least two independent experiments. **(b)** Parental PF and *TbEndoV*-RNAi cells under normal (untreated) or starvation-induced (120 min PBS) conditions were immunostained with rabbit anti-*TbEndoV* and Alexa Fluor[®] 488-conjugated goat anti-rabbit IgG. **(c)** Comparative analysis of *TbEndoV* relocalization in control and RNAi-silenced trypanosomes. *Left*, number of granules per cell in normal or starvation conditions in the wild type or *TbEndoV*-RNAi procyclic cells. Data are shown as mean (\pm s.d). At least 16 cells were analyzed for each group. *Right*, median representation of the mean granule area per cell:

box represents the interquartile range (IQR) and whiskers are maximum and minimum values. Differences in granule areas are statistically significant between untreated and starvation-induced PF cells ($p = 0.002$) and between PF and *TbEndoV*-RNAi cells in normal growth conditions or under starvation ($p = 0.03$). Unpaired two-tailed Student's *t*-test with Welch's correction; * $p < 0.05$ ** $p < 0.01$. (d) Colocalization of *TbEndoV* and *TbDhh1* in starvation stress granules. Starvation stress was induced by maintaining the trypanosomes in PBS for 120 min prior to fixation. Cells were then processed for double immunofluorescence staining using the following pairs of primary and secondary antibodies: Alexa Fluor® 594-conjugated rabbit anti-*TbEndoV* and rabbit anti-*TbDhh1*/Alexa Fluor® 488-conjugated goat anti-rabbit IgG. Untreated (no exposed to PBS) cells were used as control. Nuclear DNA and the kinetoplast were visualized by DAPI staining. The images were representative of each staining from at least two independent experiments.

may be initiated by this inosine-specific endonuclease activity. The presence of U at position 32 was somewhat detrimental for activity, which suggests that *EndoV*-mediated cleavage may be modulated by editing events.

Beyond a potential role in tRNA degradation, *TbEndoV* ability to cleave tRNAs is reminiscent of the endonucleolytic activity of yeast Rny1 and mammalian ribonuclease angiogenin. These nucleases carry out the incision of tRNAs within the anticodon loop generally as part of a stress response but in this case, tRNA cleavage is not intended to promote tRNA degradation since full-length tRNA levels are not substantially affected. Instead, tRNA-derived small RNAs themselves may function to inhibit translation or promote the degradation or repression of specific mRNAs under particular physiological conditions^{54,55}. The presence of half-tRNA molecules have been detected in *Tetrahymena*, *Aspergillus* and *Trypanosoma cruzi* following nutritional stress^{56–58} while *Saccharomyces*, *Arabidopsis* and human cells accumulate cleaved tRNAs in response to oxidative stress⁵⁹. Interestingly, *T. cruzi* secretes extracellular vesicles containing tRNA halves that may reach host mammalian cells and alter the expression of genes involved in the immune response in order to facilitate the infection⁶⁰. Although the form of tRNA processing is essentially different from the more specific *endoV*-mediated cleavage of A-to-I edited tRNAs, it raises the question as to whether cleaved tRNAs generated by the action of *TbEndoV* might perform analogous functions and participate in non-canonical regulatory pathways.

Subcellular localization analysis revealed that *TbEndoV* is primarily a cytosolic enzyme. Likewise, human *EndoV* has been localized to the cytosol but also associated to the nucleoli, suggesting an involvement in ribosomal RNA metabolism^{23,32}. Furthermore, arsenite-induced oxidative stress induces the accumulation of h*EndoV* in cytoplasmic granules where it colocalizes with polyadenylate-binding protein C1 (PABPC1)²⁴. In procyclic trypanosomes, *TbEndoV* colocalizes with *TbDhh1* in cytoplasmic stress granules upon starvation. Similarly to sodium arsenite, glucose deprivation also induces ROS production which in turn may cause harmful base deaminations in mRNAs⁶¹. While SGs are mainly involved in storage and regulation of translation of mRNAs, P bodies contain mRNAs targeted for degradation as well as factors involved in mRNA turnover. These granules are not hermetic entities neither in mammalian cells, where SGs may transiently establish physical and functional interactions with P bodies³⁵, nor in *T. brucei* where SGs and P bodies share several of their components including *TbDhh1*⁶². Likewise, it has been suggested that in *T. brucei*, some of the stress granules might arise from pre-existing P bodies as described for yeast⁶³. Although whether *TbEndoV* is a constitutive component of P bodies remains unclear, its presence in starvation-induced SGs suggest that it could be performing quality control of deaminated mRNAs and regulating the transfer of damaged transcripts to adjacent P bodies for their elimination.

We have shown that suppression of *TbEndoV* activity impairs the proliferation *in vitro* of procyclic parasites whereas bloodstream trypanosomes can still grow normally. While it has been reported that around 6% of the genes are differentially expressed between procyclic and bloodstream forms of *T. brucei*⁶⁴, *TbEndoV* appears to be equally expressed in both stages of the parasite^{64,65} and thus different enzyme requirements would not explain the obtained phenotype. It is possible that *TbEndoV* is involved in the homeostasis of specifically edited RNAs or establishes interactions with procyclic-specific proteins. Another potential factor accounting for a distinct role of *TbEndoV* in procyclics may relate to the major differences in mitochondrial metabolism between mammalian and insect-stage parasites. The identification of specific cellular substrates of the enzyme and its role in the occurrence of inosine-containing RNA will contribute to the understanding of the relevance of *TbEndoV* in parasite survival.

In summary, the data presented in this work show that *TbEndoV* exhibits incision activity preferentially upon inosine-containing RNA and appears to be needed for normal proliferation of procyclic forms where it could play a critical role in the metabolism of RNAs that are specifically required or expressed in this life stage of the parasite.

Methods

Expression and purification of wild-type and mutant endonuclease V. The endonuclease V coding sequence (Tb927.10.6860) was amplified from *T. brucei brucei* (Lister 427) genomic DNA using specific primers 5'-GCG AAT TCA TGG GTG TGG GAG AAA TGA GT-3' and 5'-GCG GAT CCT CAG CAT TCA TTT AGT TGA ATC-3'. The PCR product was cloned into pMAL-c2X vector that allows protein expression in fusion to Maltose-Binding Protein (MBP) at the N-terminus (New England Biolabs). A *TbEndoV*-D95A mutant sequence was generated using QuikChange Lightning Multi Site-Directed Mutagenesis Kit (Agilent Technologies) with the following primers: 5'-C CAC GTC GGC GGC GTT GCC ATA TCC TTT ATT CAG G-3' and 5'-C CTG AAT AAA GGA TAT GGC AAC GCC GCC GAC GTG G-3' (underlined characters indicate the codon change). MBP-*EndoV* proteins were purified by amylose affinity (New England BioLabs) followed by gel filtration chromatography. Fractions containing MBP-*EndoV* were pooled, dialyzed against storage buffer [10 mM Tris-HCl, pH 7.5, 200 mM NaCl, 1 mM DTT and 20% glycerol] and stored at -80°C .

Enzymatic assays. The 21-mer oligonucleotide substrates containing modified bases were synthesized by TriLink Biotechnologies. Oligonucleotide sequences used in all assays can be found in supplementary material (Fig. S1). All substrates were labeled at the 5'-end with [γ - 32 P]ATP (3000 Ci/mmol; Perkin Elmer) and T4 polynucleotide kinase (New England Biolabs) and purified using MicroSpin G25 columns (GE Healthcare).

In a standard reaction (10 μ L final volume), 5 fmol of [γ - 32 P]-labeled substrate were incubated in reaction buffer [20 mM Tris-HCl pH 7.5, 1 mM MnCl₂, 1% BSA, and 10 units of RNasin[®] Plus Ribonuclease Inhibitor (Promega) for RNA substrates] with increasing enzyme amounts for 1 hour at 37 °C. Reactions were terminated by adding 10 μ L of loading buffer (90% formamide, 0.1% bromophenol blue, 0.1% xylene cyanol and 50 mM EDTA) and heating at 95 °C for 5 min. Reaction products were resolved on denaturing 20% (w/v) polyacrylamide gel electrophoresis (PAGE) (19:1 acrylamide/bisacrylamide). Gels were scanned in a Typhoon 9400 scanner (Amersham Biosciences) using a Storage Phosphor Screen (Amersham Biosciences). Gel analysis to determine the percentage of cleavage was performed with Fiji software (ImageJ 1.51d).

Antibody generation. To obtain a polyclonal anti-*TbEndoV* antibody, a rabbit was immunized using soluble purified recombinant *TbEndoV*. Before injecting the antigen into the rabbit, 450 μ g of pure protein diluted in PBS was mixed with Freund's adjuvant (1:1 ratio). Antibody-containing serum was collected and affinity-purified using pure recombinant protein coupled to Affi-Gel[®] 15 resin (BioRad) following the manufacturer's instructions.

Trypanosome growth and transfection. All cell lines used in this work derive from the *Trypanosoma brucei brucei* single marker bloodstream form (BF)⁶⁶ and the *Trypanosoma brucei brucei* procyclic cell line 449 (PF)⁶⁷. Bloodstream cells were cultured at 37 °C and 5% CO₂ in HMI-9 medium supplemented with 10% (v/v) of fetal bovine serum (FBS). Procyclic parasites were cultured at 28 °C in SDM-79 medium with 10% FBS and 7.5 μ g·mL⁻¹ Haemin.

Trypanosomes were transfected by electroporation in Cytomix medium for bloodstream cells and Zimmerman medium for procyclic cells, as previously described^{66,68}. Clones were selected with appropriate selection drugs at the following concentrations: puromycin (Sigma), 0.1 μ g·mL⁻¹ (BF) and 1 μ g·mL⁻¹ (PF); hygromycin (Sigma), 5 μ g·mL⁻¹ (BF) and 50 μ g·mL⁻¹ (PF); phleomycin (Sigma), 2.5 μ g·mL⁻¹ (BF) and blasticidin (Invitrogen), 10 μ g·mL⁻¹ (PF). RNAi and *TbEndoV* expression were induced using 1 μ g·mL⁻¹ of doxycycline (Sigma).

Knock-out, RNAi and overexpression constructs. Primers sequences were obtained from GeneDB (Tb927.10.6860) and PCR amplifications were made using *T. brucei* 449 genomic DNA as template. In order to generate *TbEndoV* knockout cells, both alleles were replaced by resistance markers. Replacement cassettes were designed with resistance genes for phleomycin, blasticidin or puromycin flanked by 500 base pairs of the 3' and 5' *TbEndoV* UTRs. The 5'-UTR was amplified with primers 5'-GCG GAT CCC AAT CGT ATT TGC CCA TTT TAT TCT GAC ACA C-3' (forward) and 5'-ATG AAT TTC AGA AGA CCT TGC TGT GAT GTT CAG TTC CTG TGT TTA-3' (reverse), and the 3'-UTR with primers 5'-GCG GCC ACG GGA CGT TGA ACG CTT GTT TC-3' (forward) and 5'-GCG GAT CCG GGA GTA CAG GGA CCA GAG TAC CC-3' (reverse). BamHI restriction sites were included (underlined) to allow the linearization of the plasmid.

For the RNA interference construct, a region of *TbEndoV* of 400 bp (position 29–428 of the coding region) was amplified using the following set of primers: (forward) 5'-GCG GAT CCA AGC TTC CGC GAT AAA GTT GGA CAT G-3' and (reverse) 5'-AAC GGG CCC GCC TCC CGG AAC GCG AGG-3'. The amplification product was cloned in pGR19⁶⁹ as previously described⁷⁰.

To overexpress native *TbEndoV*, the coding sequence was amplified with primers 5'-GCC ATA TGG GTG TGG GAG AAA TGA GTG-3' and 5'-GCG GAT CCT CAG CAT TCA TTT AGT TGA ATC-3' including NdeI and BamHI restriction sites (underlined). The PCR product was cloned into pGRV23b expression vector⁴². To generate a construct for the expression of *TbEndoV* fused to a C-terminal myc tag, the coding sequence lacking the stop codon was amplified using primers 5'-GCC ATA TGG GTG TGG GAG AAA TGA GTG-3' and 5'-GCG TTA ACG CAT TCA TTT AGT TGA ATC CGT CGG A-3' including NdeI and HpaI restriction sites (underlined). The PCR product was cloned into pGRV33 expression vector⁴².

Knockout and RNAi transfected cells were analyzed by monitoring *TbEndoV* mRNA levels via quantitative PCR using the primers 5'-GAT GGT TGT GGC GTG CAC CAT CCA CTT C-3' and 5'-GAC GGT TGG GCG TAG CCG CAT AAC C-3'. Myosin levels were measured using the primers 5'-CTG CAG AAC AAG CAC GGC ATT T-3' and 5'-ACG CTC AAC AGT GGC AGT GGA A-3'.

Immunofluorescence studies. Immunofluorescence (IF) studies were performed as previously described⁷⁰. Briefly, parasites were harvested, washed twice in PBS (137 mM NaCl, 4 mM Na₂HPO₄, 1.7 mM KH₂PO₄ and 2.7 mM KCl), and fixed in 4% PFA in wash solution (PBS 1x, 0.2% Tween[®] 20) on a poly-L-lysine coated slide for 30 min. Fixed parasites were washed once in wash solution and permeabilized and blocked with 1% of NP40 in blocking solution (wash solution containing 1% blocking reagent (Roche)) during 75 min. The IF was performed by incubation with either rabbit polyclonal anti-*TbEndoV* (1:100) or mouse monoclonal anti-c-myc (Sigma, 1:100) primary antibodies in blocking solution. Alexa Fluor[®] 488 goat anti-rabbit IgG or anti-mouse IgG were used as secondary antibody (Sigma, 1:500), respectively. Preparations were finally mounted with ProLong[®] Gold Antifade Reagent with DAPI (Life Technologies). Vertical stacks of up to 40 slices (0.2 μ m steps) were captured using an Olympus wide-field microscope and Cell-R IX81 software. Images were deconvolved and pseudo-colored with Huygens Essential software (version 3.3; Scientific Volume Imaging).

For nutritional stress studies, 25 million log-phase parasites were washed twice in PBS, and starved by incubation in PBS during the indicated time. After starvation, IF was performed by incubation with rabbit polyclonal anti-*TbEndoV* (1:100) or anti-*TbDhh1* (1:100) primary antibodies in blocking solution. Alexa Fluor[®] 488

goat anti-rabbit IgG and Alexa Fluor[®] 594 goat anti-rabbit IgG were used as secondary antibody (Sigma, 1:500), respectively. To study *TbEndoV* and *TbDhh1* colocalization, anti-*TbEndoV* antibody was labeled with Alexa Fluor[®] 594 using Zenon[™] Rabbit IgG Labeling Kit (ThermoFisher) following manufacturer's instructions. After incubation with both the anti-*TbDhh1* primary antibody and Alexa Fluor[®] 488 goat anti-rabbit IgG, samples were incubated with an excess of a nonspecific primary antibody to block the secondary antibody. Preparations were then incubated with the Alexa Fluor[®] 594-conjugated anti-*TbEndoV* (1:10) during 1 hour and fixed in 4% PFA in PBS for 15 minutes.

All images were analyzed using Fiji/ImageJ software. Degree of colocalization was determined using Pearson's correlation coefficient and Manders' overlap coefficient. Both coefficients were calculated with JACoP plugin, using a manual threshold for Manders' coefficient, and given values are the mean of at least 18 cells. Overlapping of *TbDhh1* over *TbEndoV* is represented by M1, while overlapping of *TbEndoV* over *TbDhh1* is represented by M2. For the determination of the number and size of granule particles, a threshold of 0.05 microns² and 35.000 of signal intensity was manually set over Z-projection cell images (using the sum slice method).

Fluorescence-activated cell sorting (FACS) analysis and quantification of nuclei and kinetoplasts. PF cells (10⁷ cells per sample) were harvested by centrifugation and fixed with ethanol. FACS analysis with propidium iodide staining was carried out as previously described⁷⁰. To determine the number of nuclei and kinetoplasts per cell, trypanosomes (10⁶ cells per sample) were harvested by centrifugation, fixed with paraformaldehyde and mounted with ProLong[®] Gold Antifade Reagent with DAPI (Life Technologies). A Zeiss Axiophot microscope (Carl Zeiss, Inc.) was used to carry out microscopy and digital image acquisition. The quantification analysis was performed in individual cells from three independent experiments (n > 300).

Data availability. No datasets were generated or analyzed during the current study.

References

- Nishikura, K. A-to-I editing of coding and non-coding RNAs by ADARs. *Nat. Rev. Mol. Cell Biol.* **17**, 83–96 (2016).
- Ramiro, A. R. & Barreto, V. M. Activation-induced cytidine deaminase and active cytidine demethylation. *Trends Biochem. Sci.* **40**, 172–181 (2015).
- Rubio, M. A. *et al.* An adenosine-to-inosine tRNA-editing enzyme that can perform C-to-U deamination of DNA. *Proc Natl Acad Sci USA* **104**, 7821–7826 (2007).
- Rubio, M. A., Ragone, F. L., Gaston, K. W., Ibba, M. & Alfonzo, J. D. C to U editing stimulates A to I editing in the anticodon loop of a cytoplasmic threonyl tRNA in *Trypanosoma brucei*. *J. Biol. Chem.* **281**, 115–120 (2006).
- Yasui, M. *et al.* Miscoding properties of 2'-deoxyinosine, a nitric oxide-derived DNA Adduct, during translesion synthesis catalyzed by human DNA polymerases. *J. Mol. Biol.* **377**, 1015–1023 (2008).
- Lindahl, T. DNA glycosylases, endonucleases for apurinic/apyrimidinic sites, and base excision-repair. *Prog. Nucleic Acid Res. Mol. Biol.* **22**, 135–192 (1979).
- Gates, F. T. 3rd & Linn, S. Endonuclease V of *Escherichia coli*. *J. Biol. Chem.* **252**, 1647–1653 (1977).
- Yao, M., Hatahet, Z., Melamed, R. J. & Kow, Y. W. Purification and characterization of a novel deoxyinosine-specific enzyme, deoxyinosine 3' endonuclease, from *Escherichia coli*. *J. Biol. Chem.* **269**, 16260–16268 (1994).
- Demple, B. & Linn, S. On the recognition and cleavage mechanism of *Escherichia coli* endodeoxyribonuclease V, a possible DNA repair enzyme. *J. Biol. Chem.* **257**, 2848–2855 (1982).
- Yao, M. & Kow, Y. W. Cleavage of insertion/deletion mismatches, flap and pseudo-Y DNA structures by deoxyinosine 3'-endonuclease from *Escherichia coli*. *J. Biol. Chem.* **271**, 30672–30676 (1996).
- Guo, G., Ding, Y. & Weiss, B. nfi, the gene for endonuclease V in *Escherichia coli* K-12. *J. Bacteriol.* **179**, 310–316 (1997).
- He, B., Qing, H. & Kow, Y. W. Deoxyxanthosine in DNA is repaired by *Escherichia coli* endonuclease V. *Mutat. Res.* **459**, 109–114 (2000).
- Huang, J., Lu, J., Barany, F. & Cao, W. Multiple cleavage activities of endonuclease V from *Thermotoga maritima*: Recognition and strand nicking mechanism. *Biochemistry* **40**, 8738–8748 (2001).
- Yao, M. & Kow, Y. W. Strand-specific cleavage of mismatch-containing DNA by deoxyinosine 3'-endonuclease from *Escherichia coli*. *J. Biol. Chem.* **269**, 31390–31396 (1994).
- Guo, G. & Weiss, B. Endonuclease V (nfi) mutant of *Escherichia coli* K-12. *J. Bacteriol.* **180**, 46–51 (1998).
- Schouten, K. A. & Weiss, B. Endonuclease V protects *Escherichia coli* against specific mutations caused by nitrous acid. *Mutat. Res.* **435**, 245–254 (1999).
- Lee, C. C. *et al.* Endonuclease V-mediated deoxyinosine excision repair *in vitro*. *DNA Repair (Amst)* **9**, 1073–1079 (2010).
- Lee, C. C. *et al.* The excision of 3' penultimate errors by DNA polymerase I and its role in endonuclease V-mediated DNA repair. *DNA Repair (Amst)* **12**, 899–911 (2013).
- Vik, E. S. *et al.* Endonuclease V cleaves at inosines in RNA. *Nat. Commun.* **4**, 2271 (2013).
- Kiyonari, S., Egashira, Y., Ishino, S. & Ishino, Y. Biochemical characterization of endonuclease v from the hyperthermophilic archaeon. *Pyrococcus furiosus*. *J. Biochem.* **155**, 325–333 (2014).
- Mi, R., Alford-Zappala, M., Kow, Y. W., Cunningham, R. P. & Cao, W. Human endonuclease V as a repair enzyme for DNA deamination. *Mutat Res Fun Mol M* **735**, 12–18 (2012).
- Moe, A. *et al.* Incision at hypoxanthine residues in DNA by a mammalian homologue of the *Escherichia coli* antimutator enzyme endonuclease V. *Nucleic Acids Res.* **31**, 3893–3900 (2003).
- Morita, Y. *et al.* Human endonuclease V is a ribonuclease specific for inosine-containing RNA. *Nat. Commun.* **4**, 2273 (2013).
- Nawaz, M. S. *et al.* Crystal structure and MD simulation of mouse EndoV reveal wedge motif plasticity in this inosine-specific endonuclease. *Sci Rep* **6**, 24979 (2016).
- Franco, J. R., Simarro, P. P., Diarra, A. & Jannin, J. G. Epidemiology of human African trypanosomiasis. *Clin Epidemiol* **6**, 257–275 (2014).
- Huang, J., Lu, J., Barany, F. & Cao, W. Mutational analysis of endonuclease V from *Thermotoga maritima*. *Biochemistry* **41**, 8342–8350 (2002).
- Dalhus, B. *et al.* Structures of endonuclease V with DNA reveal initiation of deaminated adenine repair. *Nat. Struct. Mol. Biol.* **16**, 138–143 (2009).
- McLaughlin, P. J. & Keegan, L. P. Conflict RNA modification, host-parasite co-evolution, and the origins of DNA and DNA-binding proteins. *Biochem. Soc. Trans.* **42**, 1159–1167 (2014).
- Mi, R., Abole, A. K. & Cao, W. Dissecting endonuclease and exonuclease activities in endonuclease V from *Thermotoga maritima*. *Nucleic Acids Res.* **39**, 536–544 (2011).

30. Kuraoka, I. Diversity of Endonuclease V: From DNA Repair to RNA Editing. *Biomolecules* **5**, 2194–2206 (2015).
31. Su, A. A. & Randau, L. A-to-I and C-to-U editing within transfer RNAs. *Biochemistry (Mosc)* **76**, 932–937 (2011).
32. Fladeby, C. *et al.* The human homolog of *Escherichia coli* endonuclease V is a nucleolar protein with affinity for branched DNA structures. *PLoS One* **7**, e47466 (2012).
33. Ploubidou, A., Robinson, D. R., Docherty, R. C., Ogbadoyi, E. O. & Gull, K. Evidence for novel cell cycle checkpoints in trypanosomes: kinetoplast segregation and cytokinesis in the absence of mitosis. *J. Cell Sci.* **112**(Pt 24), 4641–4650 (1999).
34. Ono, T. & Nakabayashi, T. Studies on the effect of bleomycin on *Trypanosoma gambiense*. *Biken J* **23**, 143–155 (1980).
35. Stoecklin, G. & Kedersha, N. Relationship of GW/P-bodies with stress granules. *Adv. Exp. Med. Biol.* **768**, 197–211 (2013).
36. Cassola, A. RNA Granules Living a Post-transcriptional Life: the Trypanosomes' Case. *Curr Chem Biol* **5**, 108–117 (2011).
37. Kramer, S. *et al.* Differential localization of the two *T. brucei* poly(A) binding proteins to the nucleus and RNP granules suggests binding to distinct mRNA pools. *PLoS One* **8**, e54004 (2013).
38. Tabel, H., Kaushik, R. S. & Uzonna, J. Experimental African trypanosomiasis: differences in cytokine and nitric oxide production by macrophages from resistant and susceptible mice. *Pathobiology* **67**, 273–276 (1999).
39. Duleu, S. *et al.* Mouse strain susceptibility to trypanosome infection: an arginase-dependent effect. *J. Immunol.* **172**, 6298–6303 (2004).
40. Spletstoesser, W. D. & Schuff-Werner, P. Oxidative stress in phagocytes—“the enemy within”. *Microsc. Res. Tech.* **57**, 441–455 (2002).
41. Vonlaufen, N., Kanzok, S. M., Wek, R. C. & Sullivan, W. J. Jr. Stress response pathways in protozoan parasites. *Cell. Microbiol.* **10**, 2387–2399 (2008).
42. Castillo-Acosta, V. M. *et al.* Trypanosomes lacking uracil-DNA glycosylase are hypersensitive to antifolates and present a mutator phenotype. *Int J Biochem Cell Biol* **44**, 1555–1568 (2012).
43. Brooks, S. C., Adhikary, S., Rubinson, E. H. & Eichman, B. F. Recent advances in the structural mechanisms of DNA glycosylases. *Biochim. Biophys. Acta* **1834**, 247–271 (2013).
44. Charret, K. S. *et al.* *Trypanosoma brucei* AP endonuclease 1 has a major role in the repair of abasic sites and protection against DNA-damaging agents. *DNA Repair (Amst)* **11**, 53–64 (2012).
45. Lopez-Olmos, K. *et al.* Roles of endonuclease V, uracil-DNA glycosylase, and mismatch repair in *Bacillus subtilis* DNA base-deamination-induced mutagenesis. *J. Bacteriol.* **194**, 243–252 (2012).
46. Dedon, P. C. & Tannenbaum, S. R. Reactive nitrogen species in the chemical biology of inflammation. *Arch Biochem Biophys* **423**, 12–22 (2004).
47. Mabbott, N. A., Coulson, P. S., Smythies, L. E., Wilson, R. A. & Sternberg, J. M. African trypanosome infections in mice that lack the interferon-gamma receptor gene: nitric oxide-dependent and -independent suppression of T-cell proliferative responses and the development of anaemia. *Immunology* **94**, 476–480 (1998).
48. Sawa, T. & Ohshima, H. Nitritative DNA damage in inflammation and its possible role in carcinogenesis. *Nitric Oxide* **14**, 91–100 (2006).
49. Nguyen, T. *et al.* DNA damage and mutation in human cells exposed to nitric oxide *in vitro*. *Proc Natl Acad Sci USA* **89**, 3030–3034 (1992).
50. Christen, S., Gee, P. & Ames, B. N. Mutagenicity of nitric oxide in base pair-specific *Salmonella* tester strains: TA7000 series. *Methods Enzymol.* **269**, 267–278 (1996).
51. Pang, B. *et al.* Defects in purine nucleotide metabolism lead to substantial incorporation of xanthine and hypoxanthine into DNA and RNA. *P Natl A Sci* **109**, 2319–2324 (2012).
52. Tuorto, F. & Lyko, F. Genome recoding by tRNA modifications. *Open Biol* **6** (2016).
53. Keegan, L. P., Leroy, A., Sproul, D. & O'Connell, M. Adenosine deaminases acting on RNA (ADARs): RNA-editing enzymes. *Genome Biol.* **5**, 209 (2004).
54. Thompson, D. M. & Parker, R. Stressing out over tRNA cleavage. *Cell* **138**, 215–219 (2009).
55. Dhahbi, J. M. 5' tRNA Halves: The Next Generation of Immune Signaling Molecules. *Front Immunol* **6**, 74 (2015).
56. Lee, S. R. & Collins, K. Starvation-induced cleavage of the tRNA anticodon loop in *Tetrahymena thermophila*. *J. Biol. Chem.* **280**, 42744–42749 (2005).
57. Jochl, C. *et al.* Small ncRNA transcriptome analysis from *Aspergillus fumigatus* suggests a novel mechanism for regulation of protein synthesis. *Nucleic Acids Res.* **36**, 2677–2689 (2008).
58. Garcia-Silva, M. R. *et al.* A population of tRNA-derived small RNAs is actively produced in *Trypanosoma cruzi* and recruited to specific cytoplasmic granules. *Mol. Biochem. Parasitol.* **171**, 64–73 (2010).
59. Thompson, D. M., Lu, C., Green, P. J. & Parker, R. tRNA cleavage is a conserved response to oxidative stress in eukaryotes. *RNA* **14**, 2095–2103 (2008).
60. Garcia-Silva, M. R. *et al.* Extracellular vesicles shed by *Trypanosoma cruzi* are linked to small RNA pathways, life cycle regulation, and susceptibility to infection of mammalian cells. *Parasitol. Res.* **113**, 285–304 (2014).
61. Simons, A. L., Mattson, D. M., Dornfeld, K. & Spitz, D. R. Glucose deprivation-induced metabolic oxidative stress and cancer therapy. *J Cancer Res Ther* **5**(Suppl 1), S2–6 (2009).
62. Kramer, S. RNA in development: how ribonucleoprotein granules regulate the life cycles of pathogenic protozoa. *Wiley Interdiscip Rev RNA* **5**, 263–284 (2014).
63. Fritz, M. *et al.* Novel insights into RNP granules by employing the trypanosome's microtubule skeleton as a molecular sieve. *Nucleic Acids Res.* **43**, 8013–8032 (2015).
64. Siegel, T. N., Hekstra, D. R., Wang, X., Dewell, S. & Cross, G. A. Genome-wide analysis of mRNA abundance in two life-cycle stages of *Trypanosoma brucei* and identification of splicing and polyadenylation sites. *Nucleic Acids Res.* **38**, 4946–4957 (2010).
65. Jensen, B. C., Sivam, D., Kifer, C. T., Myler, P. J. & Parsons, M. Widespread variation in transcript abundance within and across developmental stages of *Trypanosoma brucei*. *BMC Genomics* **10**, 482 (2009).
66. Wirtz, E., Leal, S., Ochatt, C. & Cross, G. A. A tightly regulated inducible expression system for conditional gene knock-outs and dominant-negative genetics in *Trypanosoma brucei*. *Mol. Biochem. Parasitol.* **99**, 89–101 (1999).
67. Estevez, A. M., Kempf, T. & Clayton, C. The exosome of *Trypanosoma brucei*. *EMBO J.* **20**, 3831–3839 (2001).
68. Wirtz, E., Hoek, M. & Cross, G. A. Regulated processive transcription of chromatin by T7 RNA polymerase in *Trypanosoma brucei*. *Nucleic Acids Res.* **26**, 4626–4634 (1998).
69. Clayton, C. E. *et al.* Down-regulating gene expression by RNA interference in *Trypanosoma brucei*. *Methods Mol Biol* **309**, 39–60 (2005).
70. Castillo-Acosta, V. M., Estevez, A. M., Vidal, A. E., Ruiz-Perez, L. M. & Gonzalez-Pacanowska, D. Depletion of dimeric all-alpha dUTPase induces DNA strand breaks and impairs cell cycle progression in *Trypanosoma brucei*. *Int J Biochem Cell Biol* **40**, 2901–2913 (2008).

Acknowledgements

We thank Dr. Mark Carrington for providing the anti-*TbDhh1* antibody. This work was supported by the Junta de Andalucía [BIO-199], the Plan Nacional de Investigación Científica, Instituto de Salud Carlos III-Subdirección General de Redes y Centros de Investigación Cooperativa-Red de Investigación Cooperativa en Enfermedades Tropicales (RICET FIS Network: RD12/0018/0017), the Plan Nacional (SAF2016-79957-R) and the FEDER funds from the EU.

Author Contributions

D.G.P. and A.E.V. conceived the project; D.G.P., G.P.M., L.M.R.P., A.E.V. and D.G.C. designed the experiments and analyzed the data; D.G.C. performed protein purifications, enzymatic assays, cell lines construction and characterization; D.G.C., G.P.M. and A.M.E. contributed to the immunolocalization studies; D.G.C., L.M.R.P., A.E.V. and D.G.P. wrote the manuscript; all the authors revised the manuscript.

Additional Information

Supplementary information accompanies this paper at doi:[10.1038/s41598-017-08910-1](https://doi.org/10.1038/s41598-017-08910-1)

Competing Interests: The authors declare that they have no competing interests.

Publisher's note: Springer Nature remains neutral with regard to jurisdictional claims in published maps and institutional affiliations.



Open Access This article is licensed under a Creative Commons Attribution 4.0 International License, which permits use, sharing, adaptation, distribution and reproduction in any medium or format, as long as you give appropriate credit to the original author(s) and the source, provide a link to the Creative Commons license, and indicate if changes were made. The images or other third party material in this article are included in the article's Creative Commons license, unless indicated otherwise in a credit line to the material. If material is not included in the article's Creative Commons license and your intended use is not permitted by statutory regulation or exceeds the permitted use, you will need to obtain permission directly from the copyright holder. To view a copy of this license, visit <http://creativecommons.org/licenses/by/4.0/>.

© The Author(s) 2017